NANO MICRO small

Supporting Information

for *Small,* DOI: 10.1002/smll.202206774

The Impact of Carbon Nanotube Length and Diameter on their Global Alignment by Dead-End Filtration

*Christian Rust, Pavel Shapturenka, Manuel Spari, Qihao Jin, Han Li, Andreas Bacher, Markus Guttmann, Ming Zheng, Tehseen Adel, Angela R. Hight Walker, Jeffrey A. Fagan, and Benjamin S. Flavel**

Supporting Information

The Impact of Carbon Nanotube Length and Diameter on their Global Alignment by Dead-End Filtration

*Christian Rust, Pavel Shapturenka, Manuel Spari, Qihao Jin, Han Li, Andreas Bacher, Markus Guttmann, Ming Zheng, Tehseen Adel, Angela R. Hight Walker, Jeffrey A. Fagan & Benjamin S. Flavel**

Certain equipment, instruments, or materials are identified in this paper in order to adequately specify the experimental details. Such identification does not imply recommendation by the National Institute of Standards and Technology (NIST) nor does it imply the materials are necessarily the best available for the purpose. Except where specified otherwise, uncertainty in this contribution is reported as one standard deviation.

DLVO Calculations:

Φ_{TOT} with respect to the distance *z* to the surface was calculated for an individual single-wall carbon nanotube (SWCNT) following the approach of Wu *et al.*[1] with the SWCNT parallel to the membrane surface ($\varphi = \frac{\pi}{2}$), as this orientation yields the lowest potential possible and is thus most plausible.

Consistent parameters for all DLVO calculations shown in Figure 7:
T = 298.15 K, temperature in Kelvin
A = 9.81 × 10^{-21} J, Hamaker constant[1a]
R = 0.04 nm, thickness of the cylinder wall and approximated by the thickness of graphene.
κ^{-1} = 2.9 nm, Debye-length (inverse Debye-Hückel parameter) for I = 10 mmol L^{-1}, T = 298 K.
$\epsilon_0\epsilon_r$: permittivity of water at T = 298 K
γ_2 = -67 mV, surface charge of a pristine membrane at pH 7
ν = 1, valence
k = 1.38066 × 10^{-23} J/K, Boltzmann constant
Parameters for single curves calculation Figure 7 (A, B):
$d_{\mathrm{t\,EA-SWCNT}}$ = 1.4 nm, average SWCNT diameter.
$d_{\mathrm{t\,CoMoCAT}}$ = 0.76 nm, average SWCNT diameter.
γ_1, surface charge of the nanotube
The surface charge has been approximated using the zeta potential derived from the Zetasizer measurements (see Methods section), which can be found in Figure 1 (C) for the length sorted electric arc (EA)-SWCNT fractions and Figures S17 and S18 for the unsorted and length-sorted cobalt-molybdenum catalyst (CoMoCAT)-SWCNTs.

Parameters for SWCNT length (L) and d_t dependence calculation Figure 7 (C,D):
Range of diameter of the SWCNTd_t: 0.5 nm to 2.75 nm, 0.05 nm intervals
Range of distance to the surface, z: 1 nm to 50 nm, 0.25 nm intervals
Range of length L: 50 nm to 5000 nm, 10 nm intervals
Range of the surface potential of the SWCNT, γ_1: -10 mV to -40 mV, -10 mV intervals
Threshold for secondary minimum: -0.075 kT (I = 0.01 mol L^{-1})

Parameters for SWCNT length (L) and d_t dependence calculation Figure S31 (A,B):
Similar to the ones mentioned above, with the exception of the ionic strength and the corresponding thresholds for the secondary minimum:
-1.102 kT (I = 100 mmol L^{-1}), -0.075 kT (I = 10 mmol L^{-1}), and -0.058 kT (I = 1 mmol L^{-1}).

Fitting parameters for the L and d_t relationship are based on the inverse length plot shown in Figure 7 (D). The linear fit can be written as:

$$L^{-1} = m_{\zeta SWCNT} d_t + b_{\zeta SWCNT} \qquad (1)$$

$$L = \frac{1}{m_{\zeta SWCNT} d_t + b_{\zeta SWCNT}} \qquad (2)$$

All fits had fitting errors below 1 %. The slope and intercept vary with the zeta potential of the SWCNT as shown below:

$m_{\zeta SWCNT=-40mV}$ = 1.541 × 10^{12} m^{-2}, $b_{\zeta SWCNT=-40mV}$ = -0.083 × 10^3 m^{-1}
$m_{\zeta SWCNT=-30mV}$ = 1.633 × 10^{12} m^{-2}, $b_{\zeta SWCNT=-30mV}$ = -0.089 × 10^3 m^{-1}
$m_{\zeta SWCNT=-20mV}$ = 1.786 × 10^{12} m^{-2}, $b_{\zeta SWCNT=-20mV}$ = -0.098 × 10^3 m^{-1}

$m_{\zeta SWCNT=-10mV}$= 2.122 × 10^{12} m^{-2}, $b_{\zeta SWCNT=-20mV}$= -0.119 × 10^{3} m^{-1}

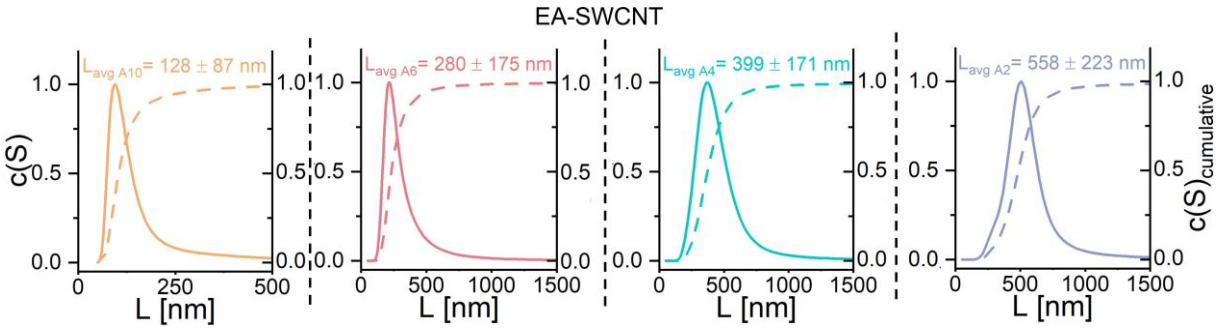

Figure S1. Length determination of the EA-SWCNT fractions by analysis of their sedimentation coefficient as measured with an analytical ultracentrifuge (AUC). SWCNT length as a function of sedimentation coefficient is calculated using previously determined nanotube parameters,[2] measured solution parameters (*e.g.*, solution viscosity and density) and hydrodynamic theory for rod length.[3] Estimated number-basis distributions are calculated by assuming a constant absorbance per unit length of EA-SWCNT, dividing the (absorbance) signal-weighted sedimentation coefficient distribution by the length at each value (as the dependence of signal per length is linear), and then calculating the distribution.

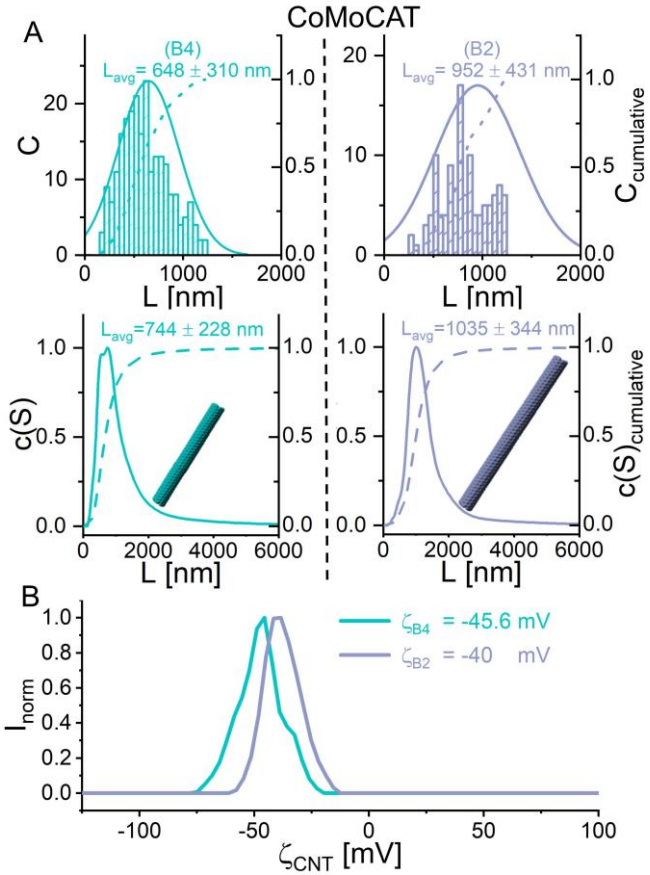

Figure S2. Average length of the CoMoCAT fractions determined from (A) atomic force microscopy (AFM) topographies and (B) AUC sedimentation curves. (C) Zeta potential of the fractions dispersed in 0.4 g/L (0.04 %) DOC and at a SWCNT concentration of 8 μg mL^{-1}.

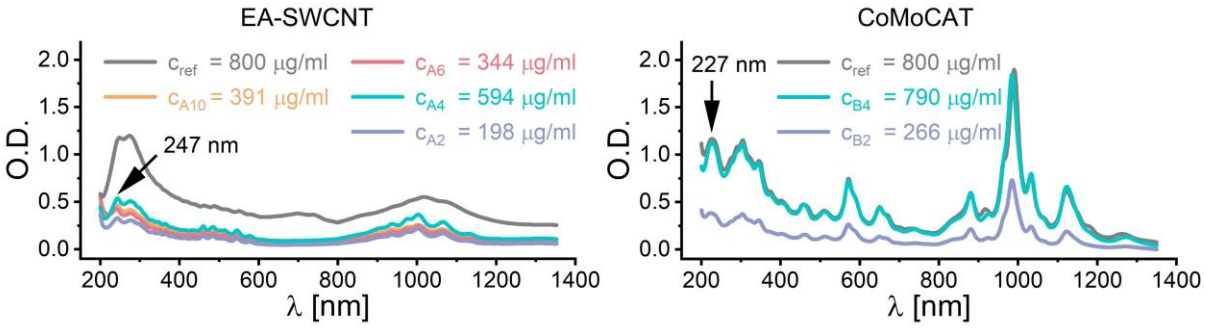

Figure S3. Absolute absorbance spectra of the SWCNT samples after dilution plotted as optical density (O.D.) as a function of wavelength (λ). The concentration of each fraction was estimated using the π-plasmon peak (274 nm for EA-SWCNTs and 227 nm for CoMoCAT SWCNTs). Enrichment of the dispersions was performed by repeatedly filtering the dispersions onto a microfiltration membrane (300 kDa, Biomax polyethersulfone, Merck Millipore) similar to our previous study.[1b] The DOC-surfactant concentration of the enriched samples was 1 %. This allowed us to adjust the concentration of all intermediate stock solutions to 8 µg mL^{-1} SWCNTs and 0.04 % DOC. For filtration 1 mL, 1.5 mL or 3 mL of this intermediate solution was diluted to 20 mL with H_2O (d), leading to 8 µg (0.4 µg mL^{-1} SWCNTs, 0.02 % DOC), 12 µg (0.6 µg mL^{-1} SWCNTs, 0.03 % DOC), or 24 µg (1.2 µg mL^{-1} SWCNTs, 0.06 % DOC) being deposited onto the membrane, respectively.

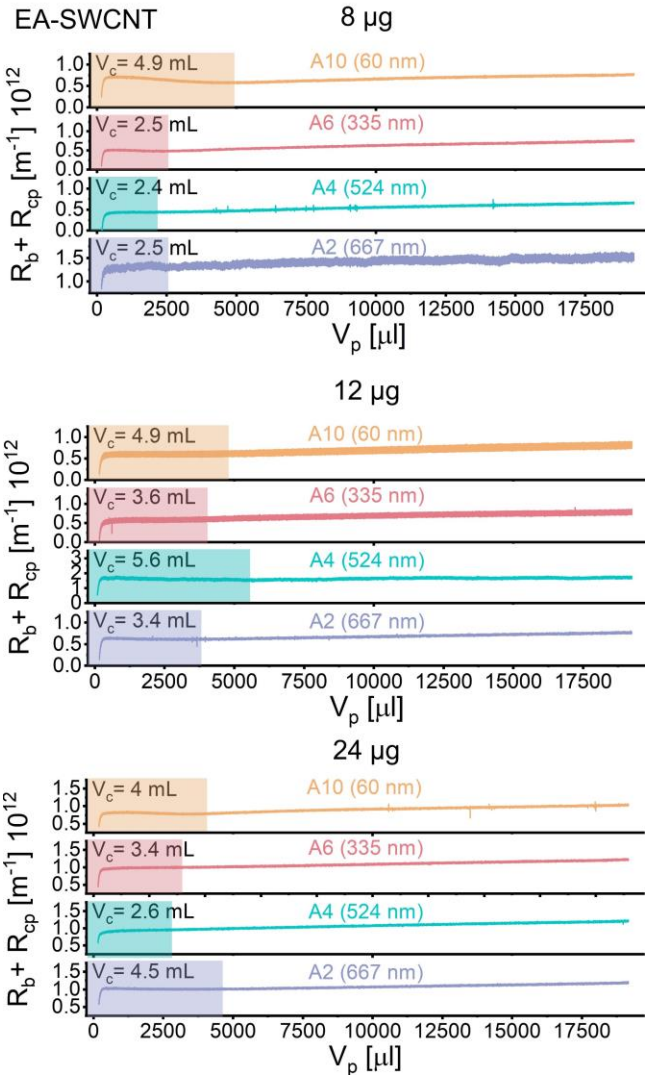

Figure S4. Evolution of the filtration resistance, which is the sum of the blocking resistance (R_b) (the accumulation of mass on the membrane) and resistance from concentration polarization (R_{cp}), obtained by subtracting the membrane resistance R_m = 2.43×10^{12} m^{-1}[1b] from the total resistance (R_{tot}) as measured during the slow filtration step (volume rate = 100 µL min^{-1}) for total SWCNT masses of 8 µg, 12 µg and 24 µg. Each mass was dispersed in 20 mL of H_2O.

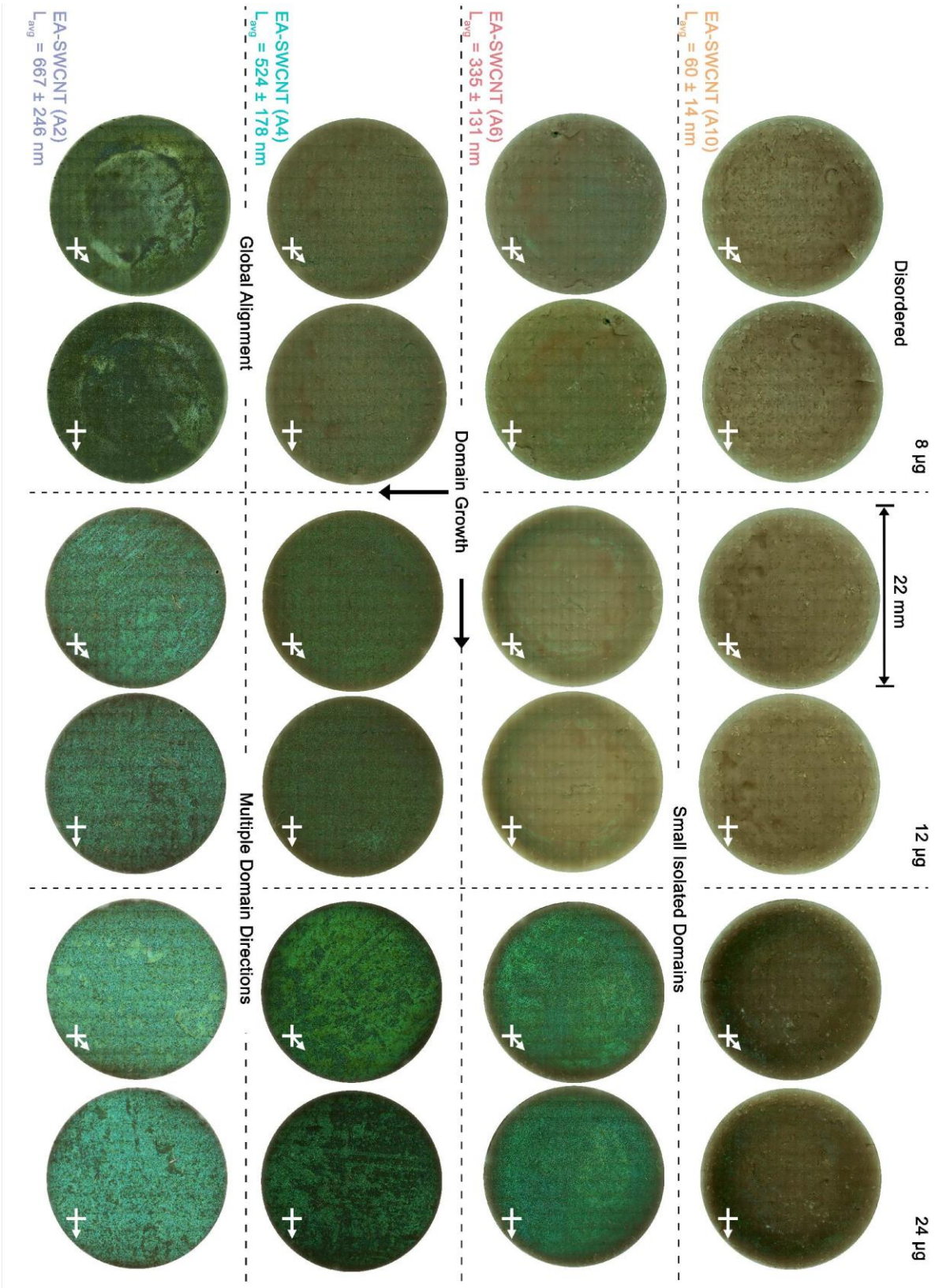

Figure S5. Cross polarized microscopy of EA-SWCNT films from length fractions A10 – A2 in the bright (45°) and dark (0°) orientation. Images were recorded with the SWCNT film on the polycarbonate track-etched (PCTE) membrane.

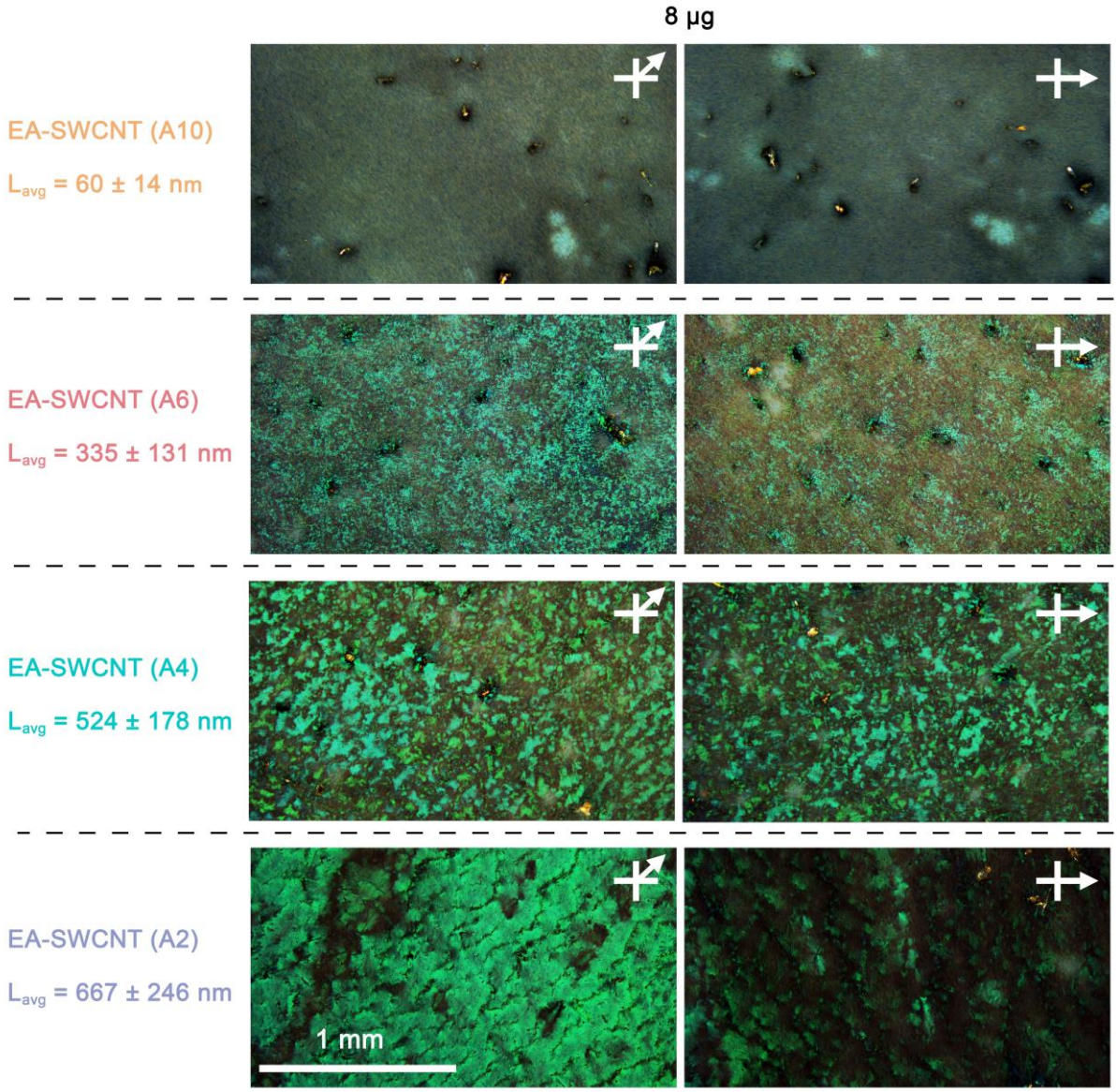

Figure S6. Cross polarized microscopy of EA-SWCNT films from 8 µg of the length sorted fractions A10 through A2 in the bright (45°) and dark (0°) orientation. Images were recorded with the SWCNT film on the PCTE membrane.

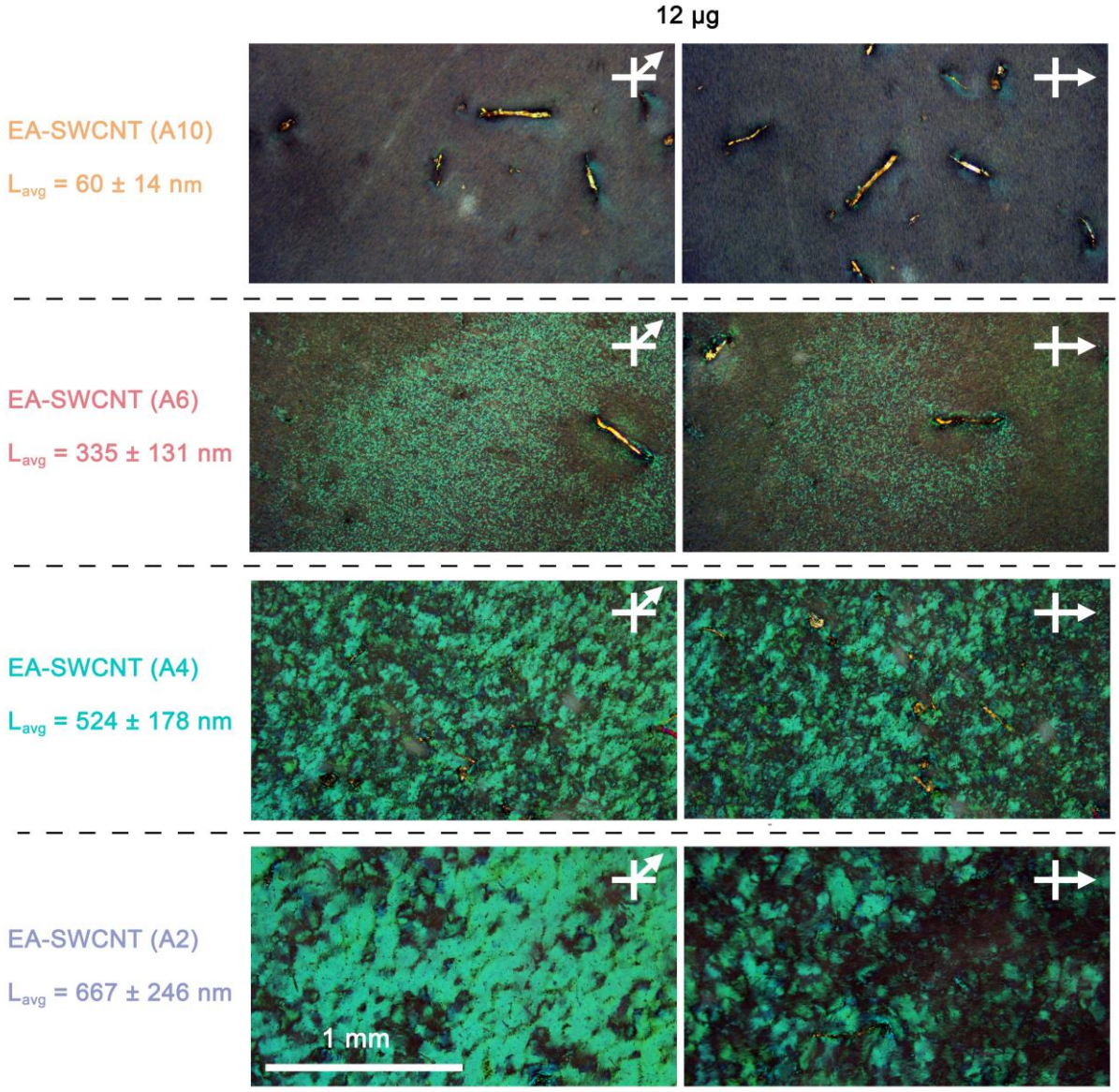

Figure S7. Cross polarized microscopy of EA-SWCNT films from 12 µg of the length sorted fractions A10 through A2 in the bright (45°) and dark (0°) orientation. Images were recorded with the SWCNT film on the PCTE membrane.

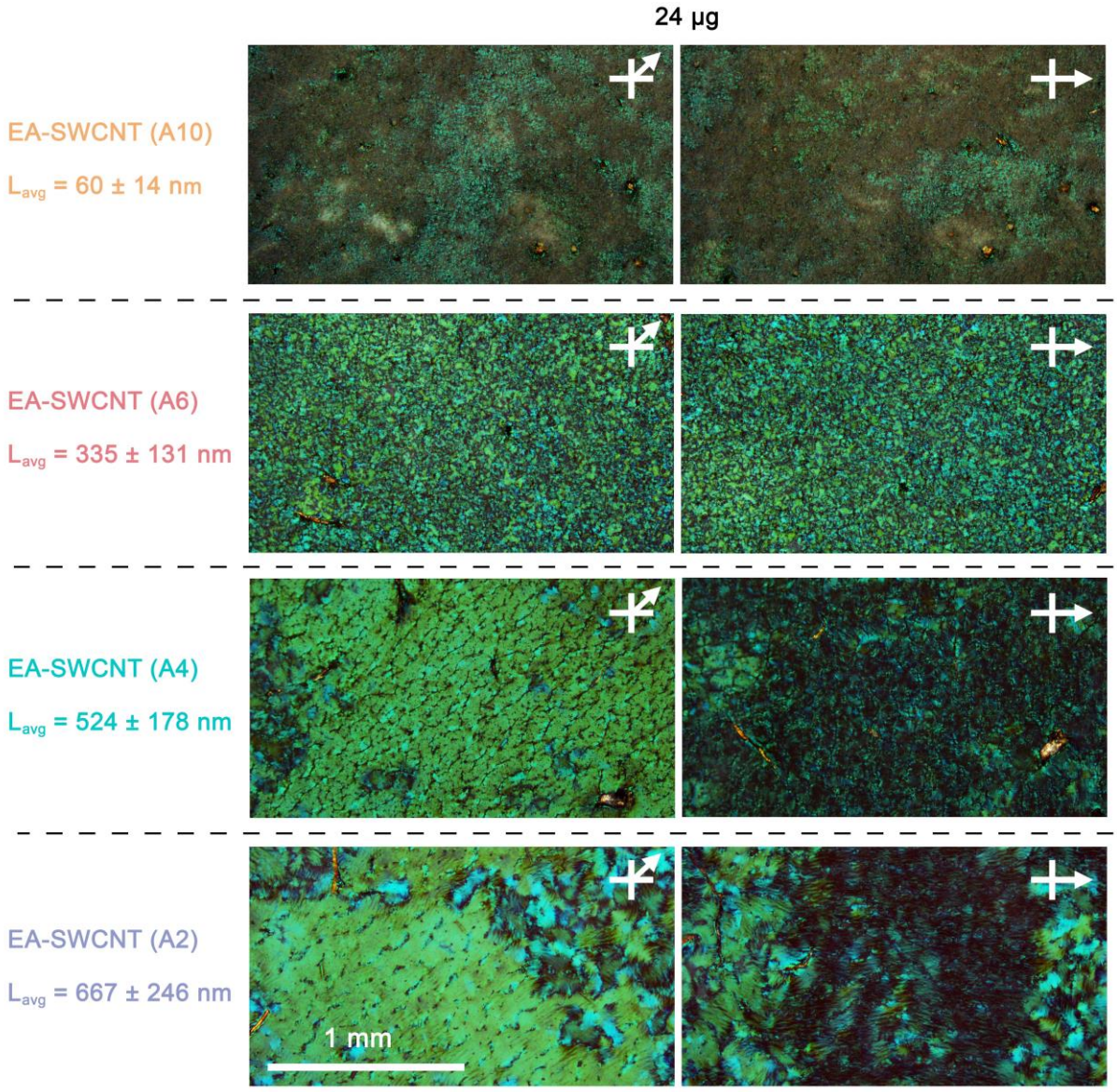

Figure S8. Cross polarized microscopy of EA-SWCNT films from 24 µg of the length sorted fractions A10 through A2 in the bright (45°) and dark (0°) orientation. Images were recorded with the SWCNT film on the PCTE membrane.

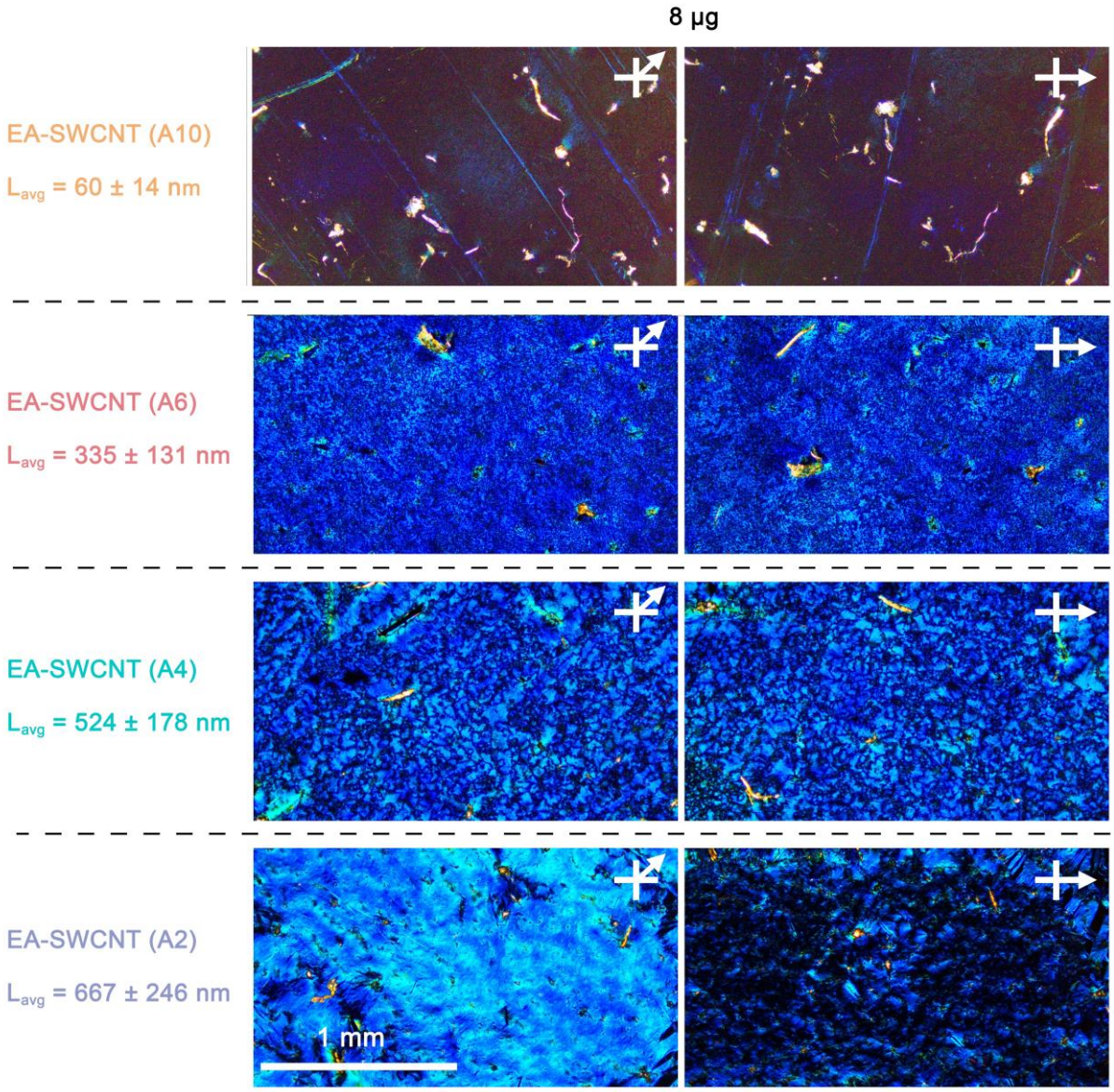

Figure S9. Cross polarized microscopy of the back side (membrane contact side) of the EA-SWCNT films from 8 µg of the length sorted fractions A10 through A2 in the bright (45°) and dark (0°) orientation. Images were recorded after transfer of the SWCNT film to a silicon wafer.

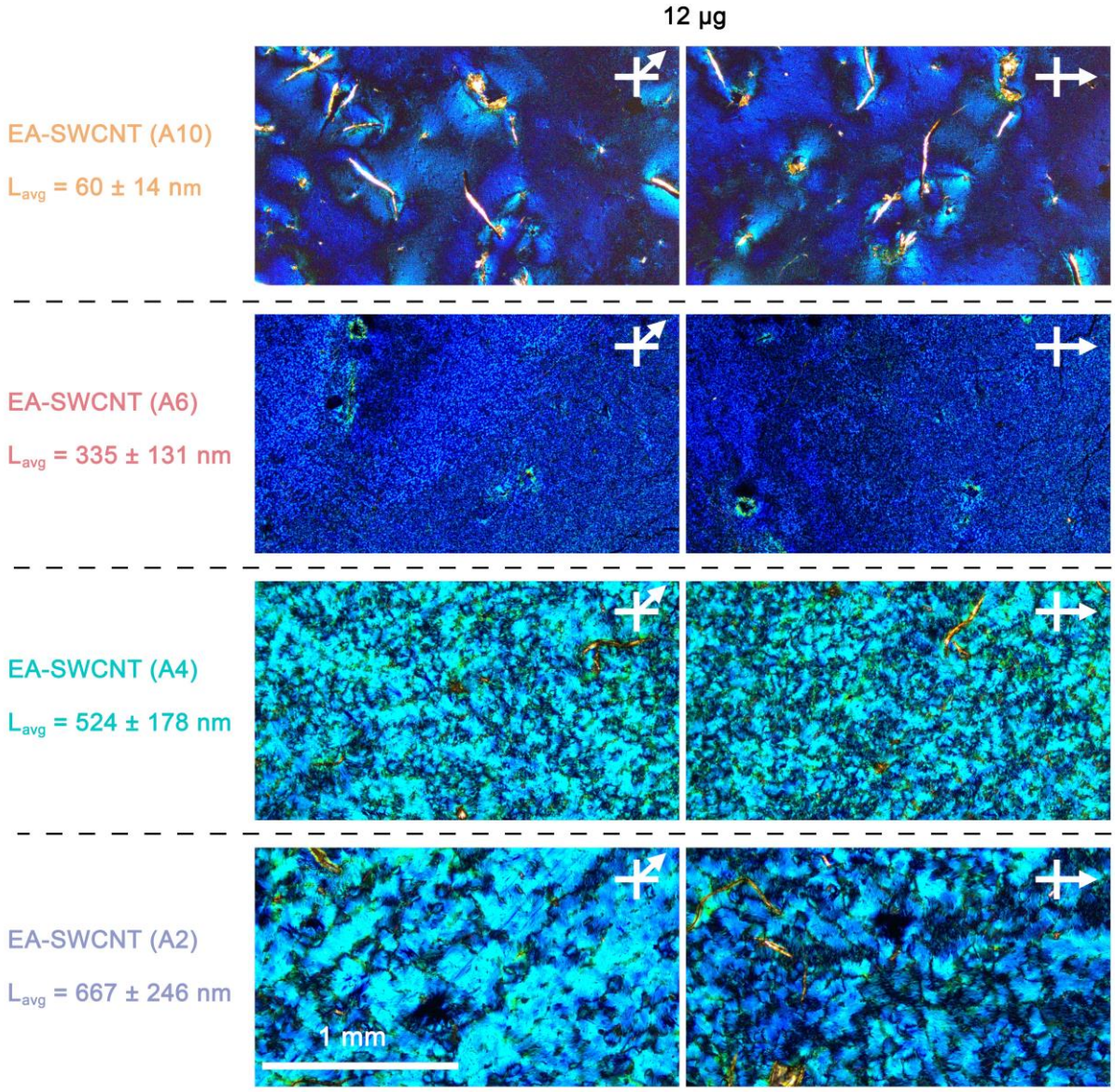

Figure S10. Cross polarized microscopy of the back side (membrane contact side) of the EA-SWCNT films from 12 µg of the length sorted fractions A10 through A2 in the bright (45°) and dark (0°) orientation. Images were recorded after transfer of the SWCNT film to silicon.

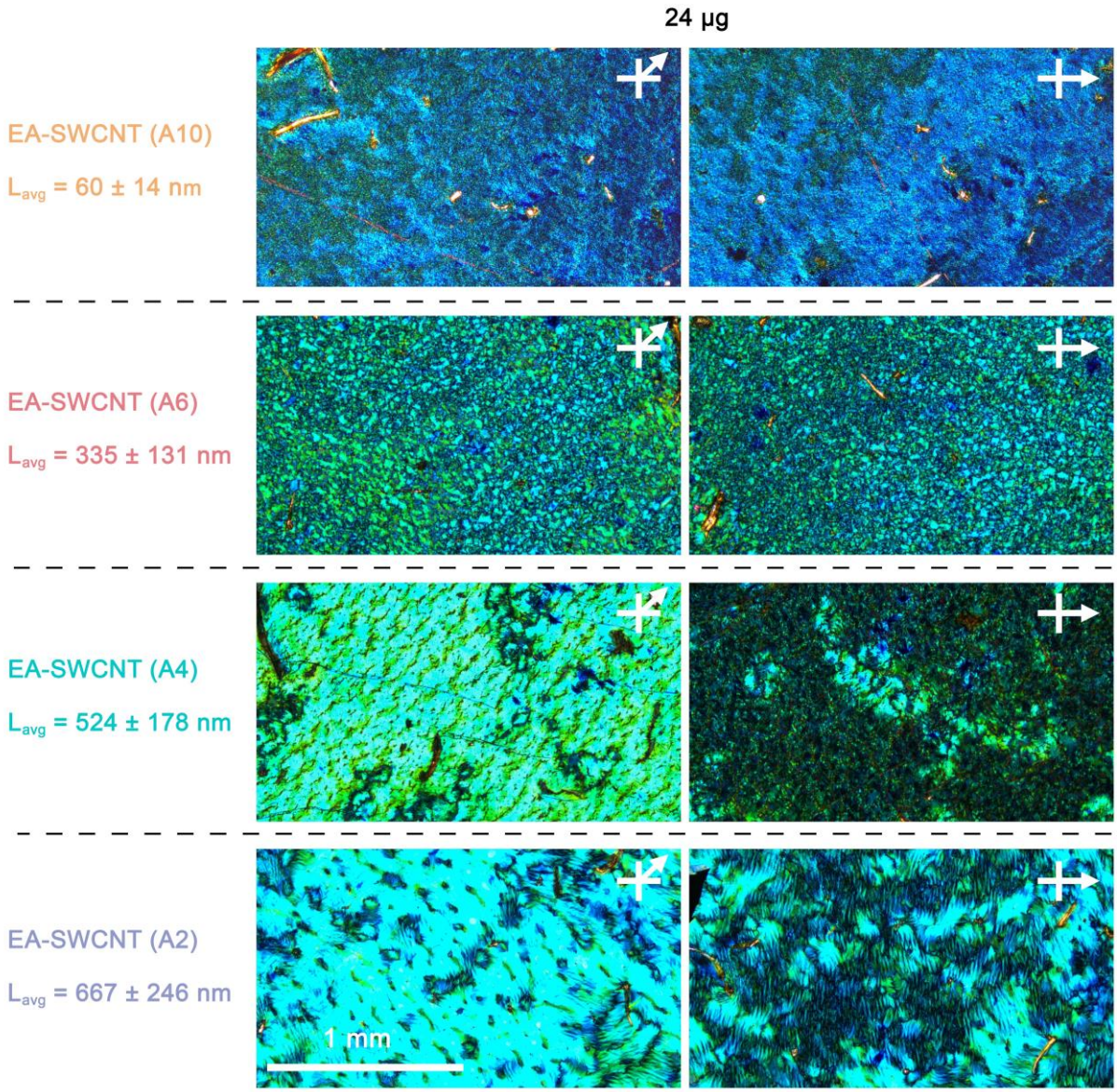

Figure S11. Cross polarized microscopy of the back side (membrane contact side) of the EA-SWCNT films from 12 µg of the length sorted fractions A10 through A2 in the bright (45°) and dark (0°) orientation. Images were recorded after transfer of the SWCNT film to silicon.

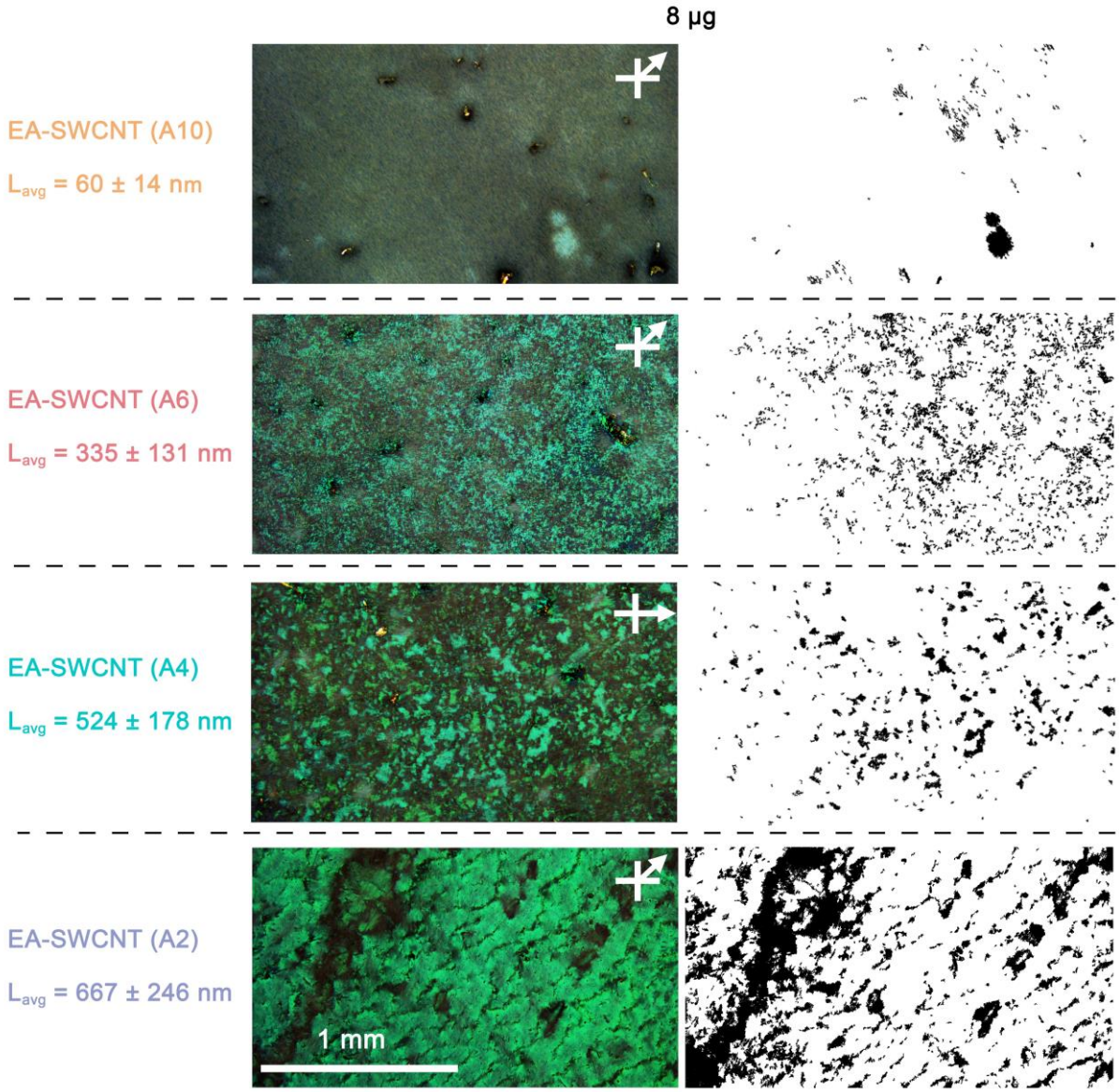

Figure S12. Cross polarized microscopy of EA-SWCNT films from 8 µg of the length sorted fractions A10 through A2 in the bright (45°) or dark (0°) orientation and maps of the detected grains (A10 through A4) or grain boundaries (A2) using machine vision.[1b]

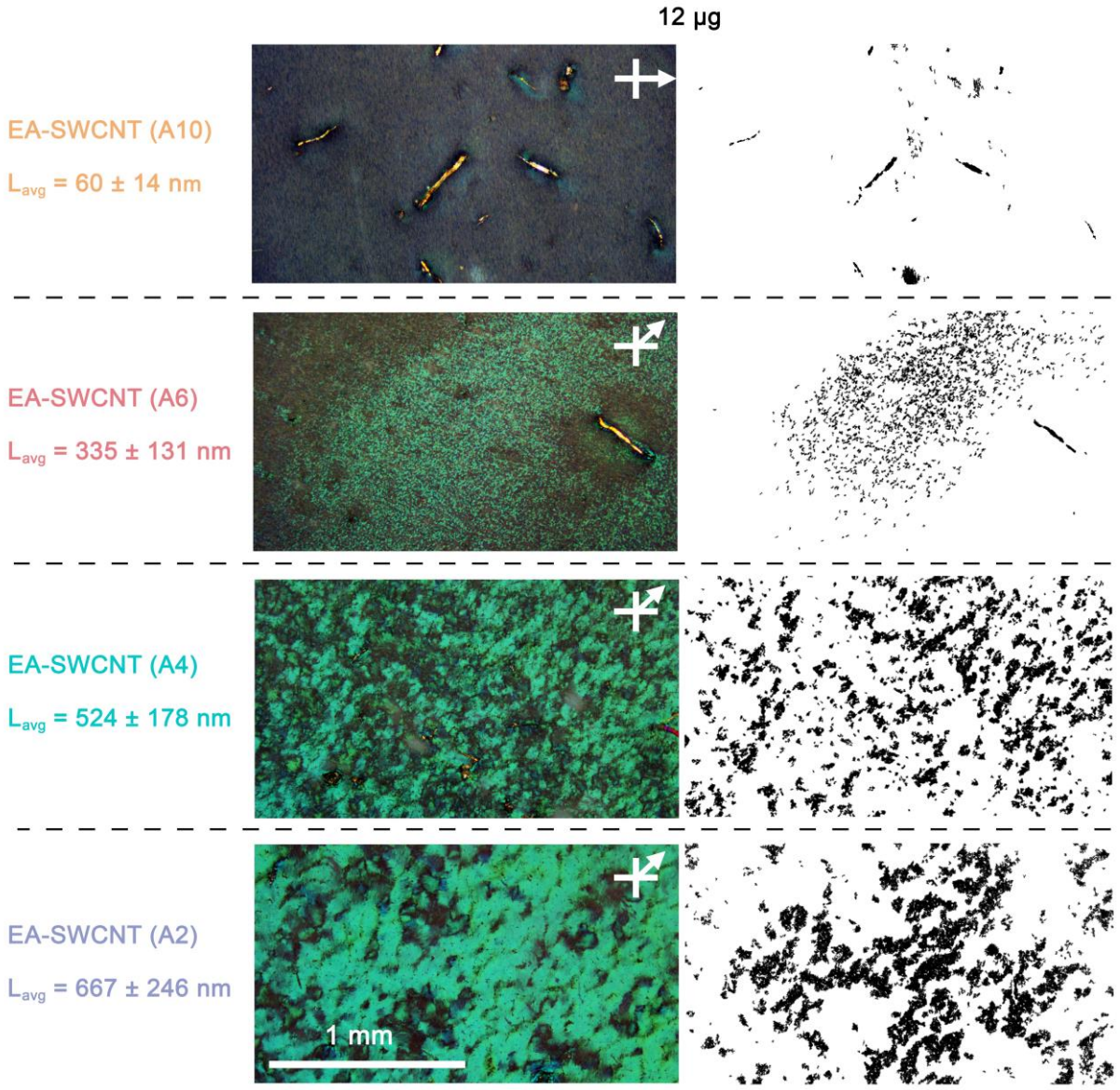

Figure S13. Cross polarized microscopy of EA-SWCNT films from 12 µg of the length sorted fractions A10 – A2 in the bright (45°) or dark (0°) orientation and maps of the detected grains using machine vision. The elongated elements seen in A10 and A6 have been neglected from the evaluation and are attributed to sample contamination.

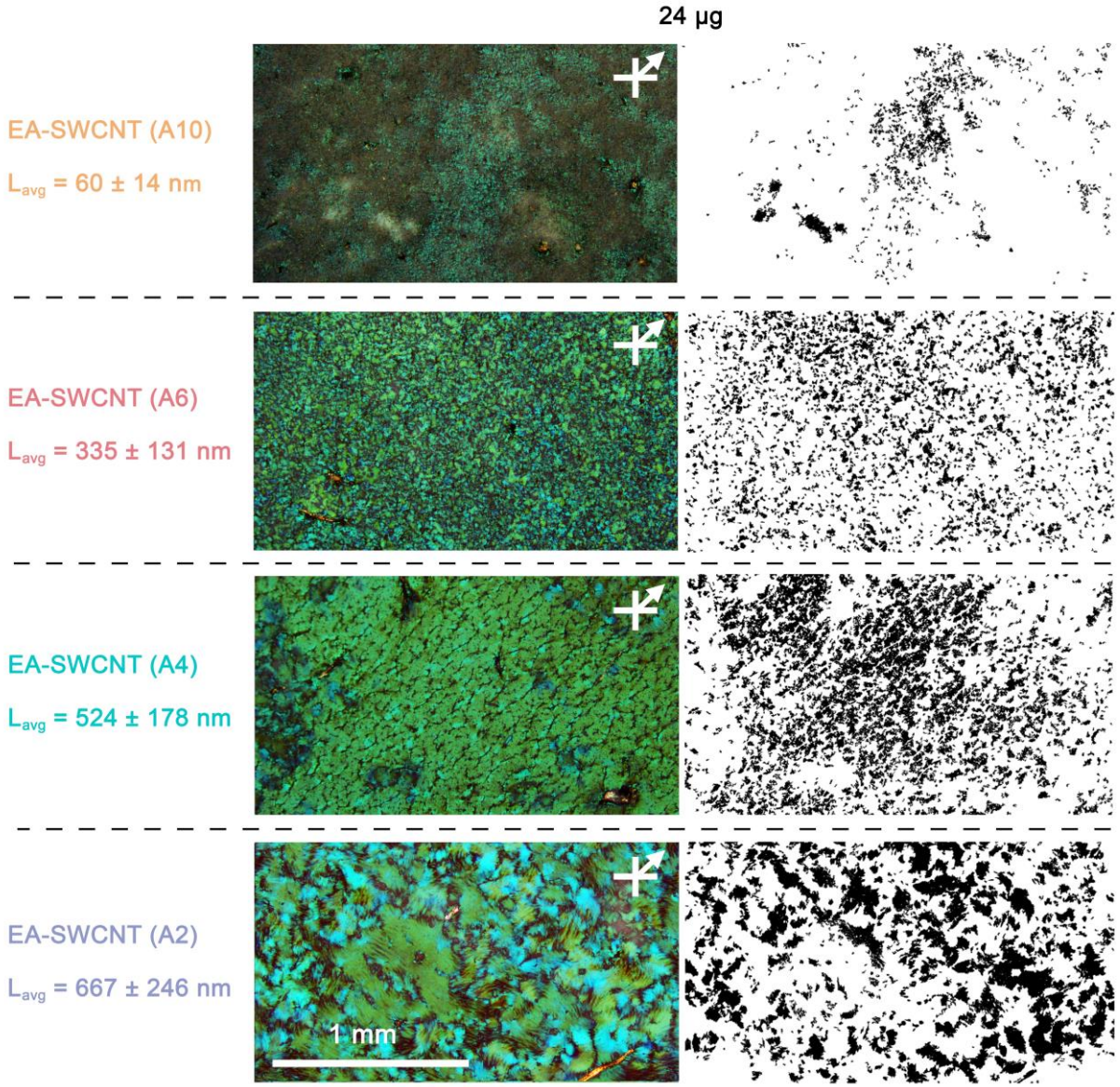

Figure S14. Cross polarized microscopy of EA-SWCNT films from 24 µg of the length sorted fractions A10 – A2 in the bright (45°) or dark (0°) orientation and maps of the detected grains (A10 – A4) or grain boundaries (A2) using machine vision.[1b]

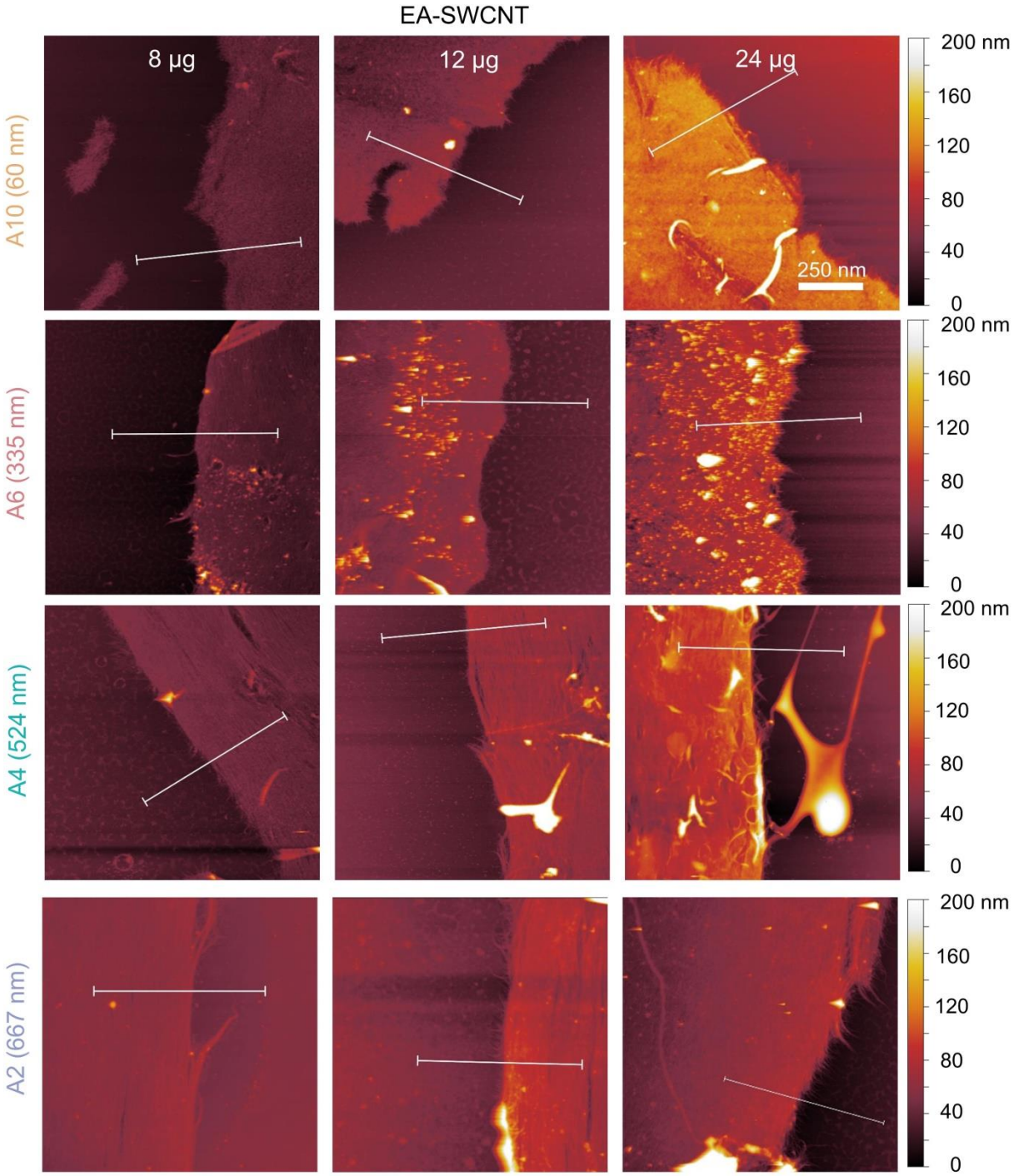

Figure S15. AFM Topographies measured in tapping mode of EA-SWCNT films made from the length sorted fractions A10 – A2 at masses of 8 µg, 12 µg and 24 µg. Images were recorded after transfer of the SWCNT film to a silicon substrate and the thickness measurement in Figure S16 is indicated by the white bar

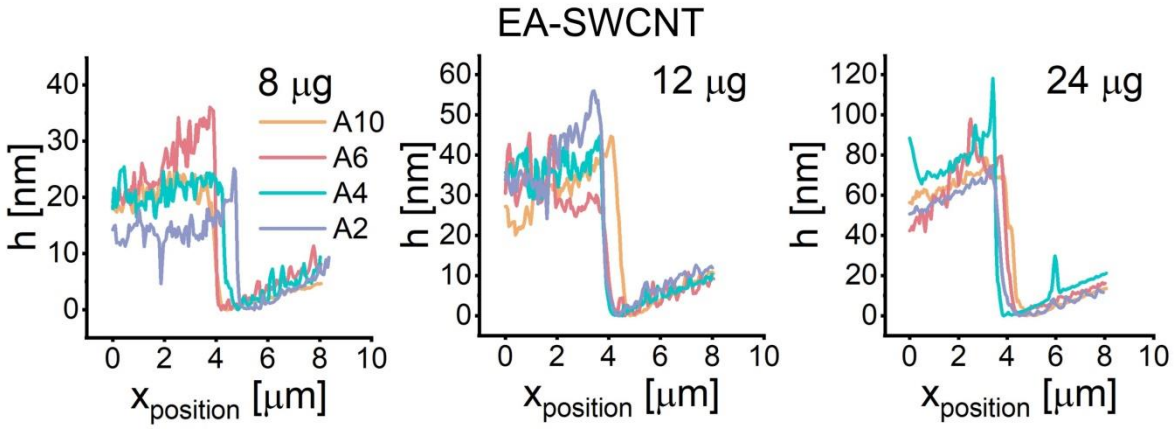

Figure S16. Evaluation of the film thickness from height (h) measurements shown in Figure S15. The average film height was determined by the step height between the substrate and the film and is plotted in Figure 4 (D).

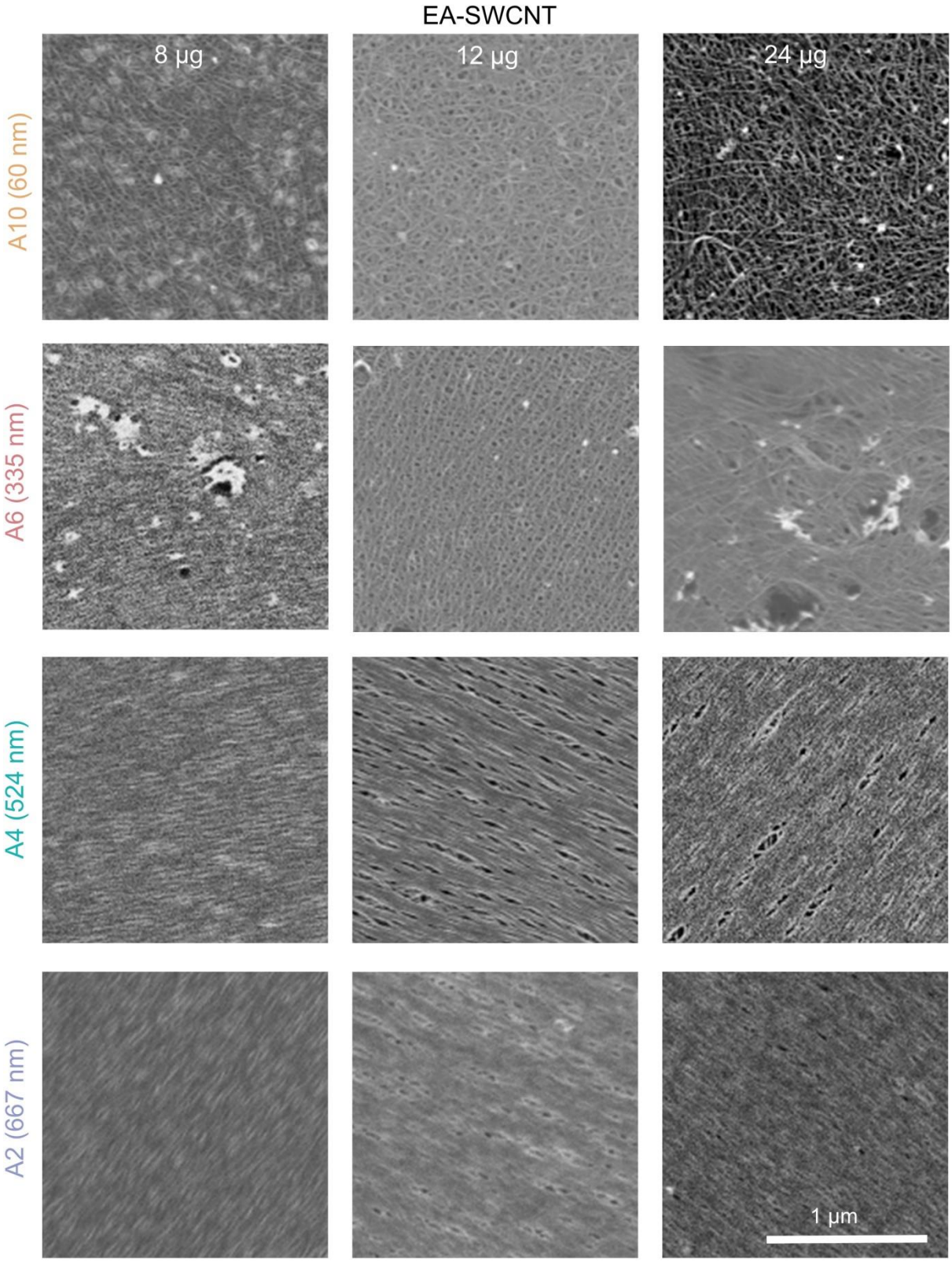

Figure S17. Scanning electron microscopy (SEM) images of EA-SWCNT films transferred to silicon. The films made from short SWCNTs (A10) mainly consist of disordered regions, A6 shows nematic regions and smaller domains and A4 and A2 consist of aligned domains, and are indistinguishable from each on this length scale

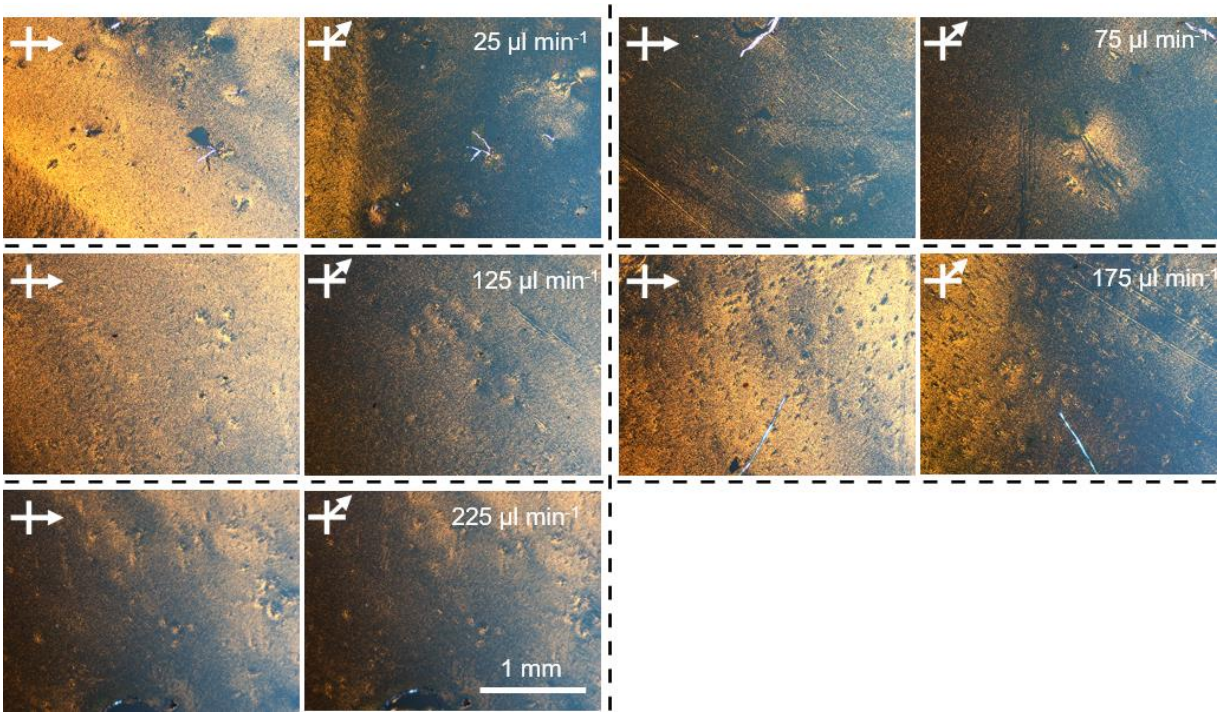

Figure S18. Optimization of the initial volume-rate for unsorted CoMoCAT-SWCNTs filtered onto an 80 nm membrane with a final push step of 500 µL min^{-1}. Cross polarized microscopy mages were recorded after transfer of the SWCNT film to a silicon wafer. The film filtered at 125 µL min^{-1} shows a slight tendency towards global alignment (greater contrast between bright and dark positions) but a closer inspection in Figure S19 reveals 10×10 µm² domains separated by large grain boundaries with a size similar to the domains.

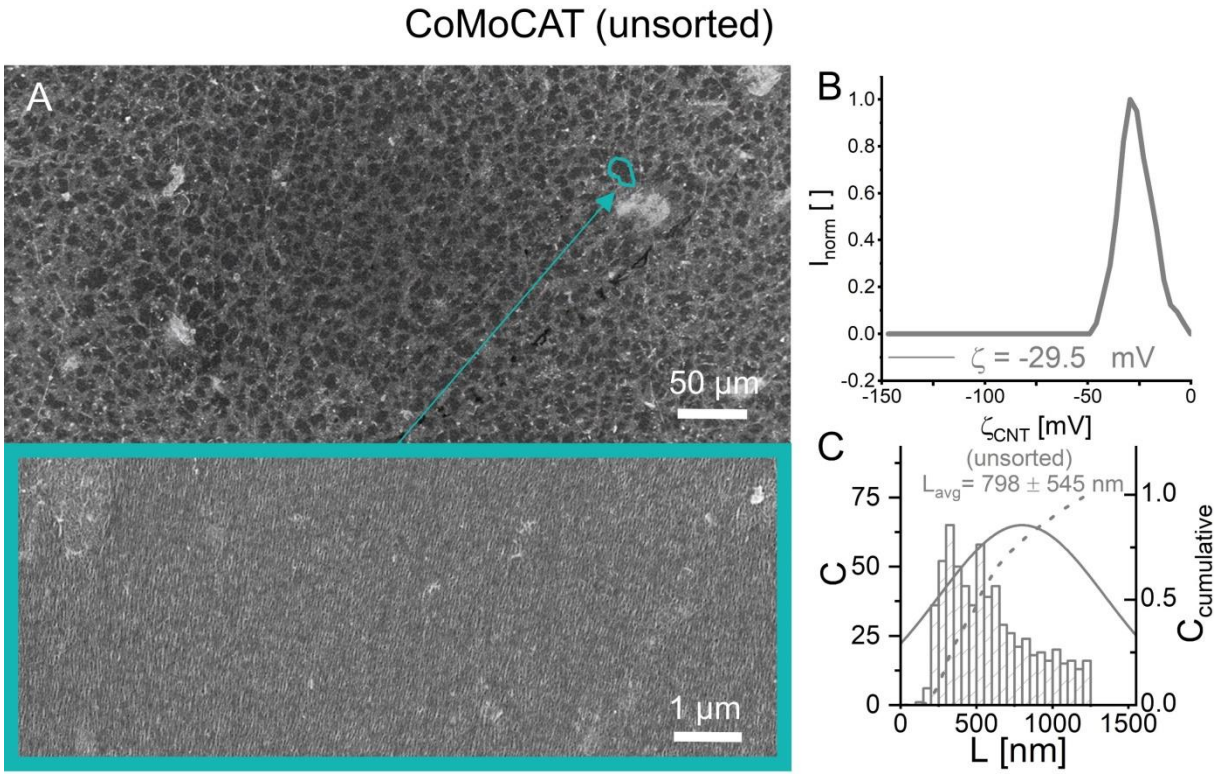

Figure S19. (A) SEM images of the CoMoCAT film filtered at 125 µL min^{-1} and shown in Figure S18. The film mainly consisted of small-sized domains with equally-sized grain boundaries. (B) Zeta potential of the CoMoCAT dispersion (8 µg $µL^{-1}$) in 0.04 % DOC. (C) The average length of the SWCNTs as determined from AFM topographies.

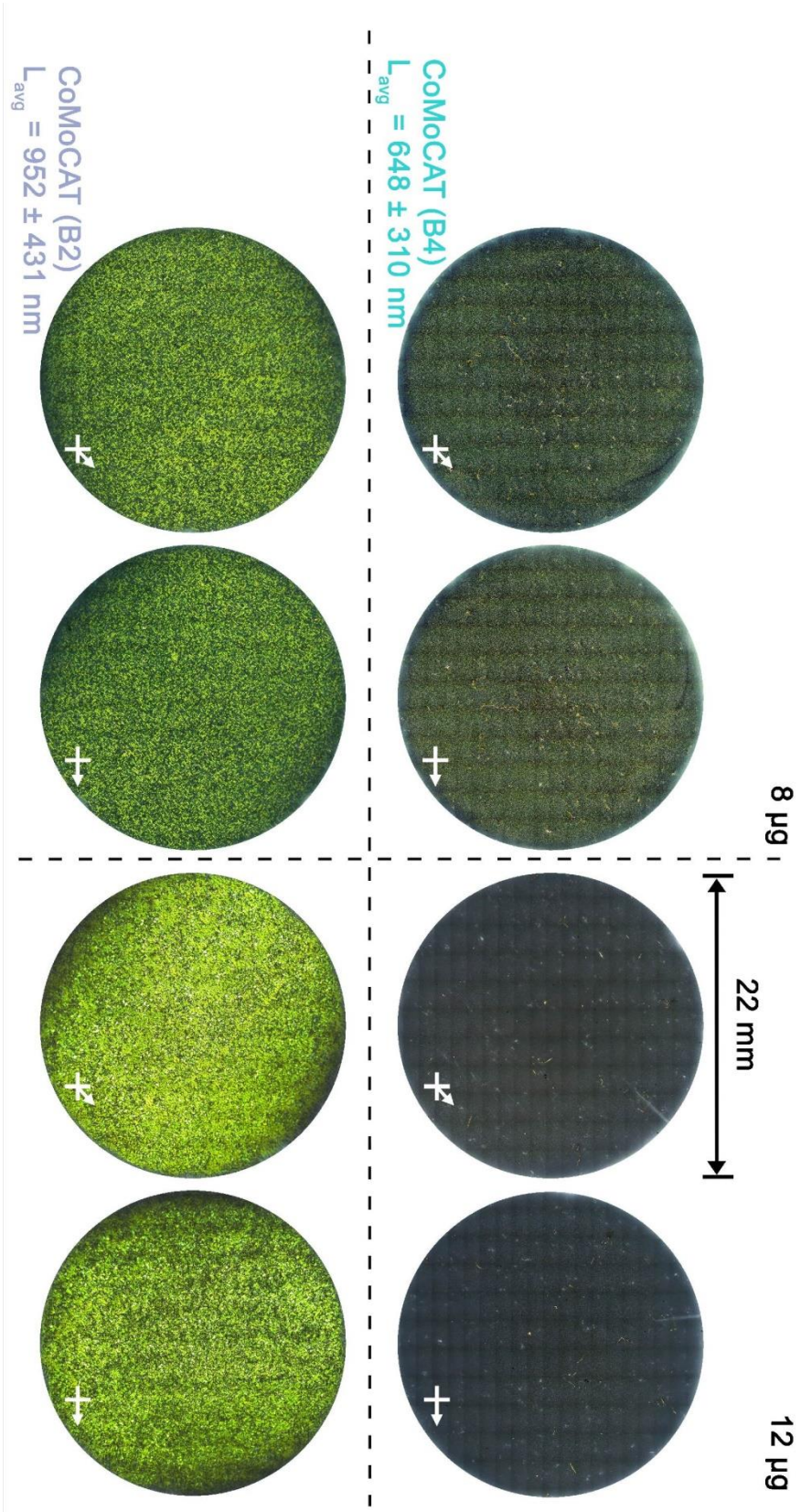

Figure S20. Cross polarized microscopy of CoMoCAT films from length fractions B2 and B4 in the bright (45°) and dark (0°) orientation and on pristine membranes.

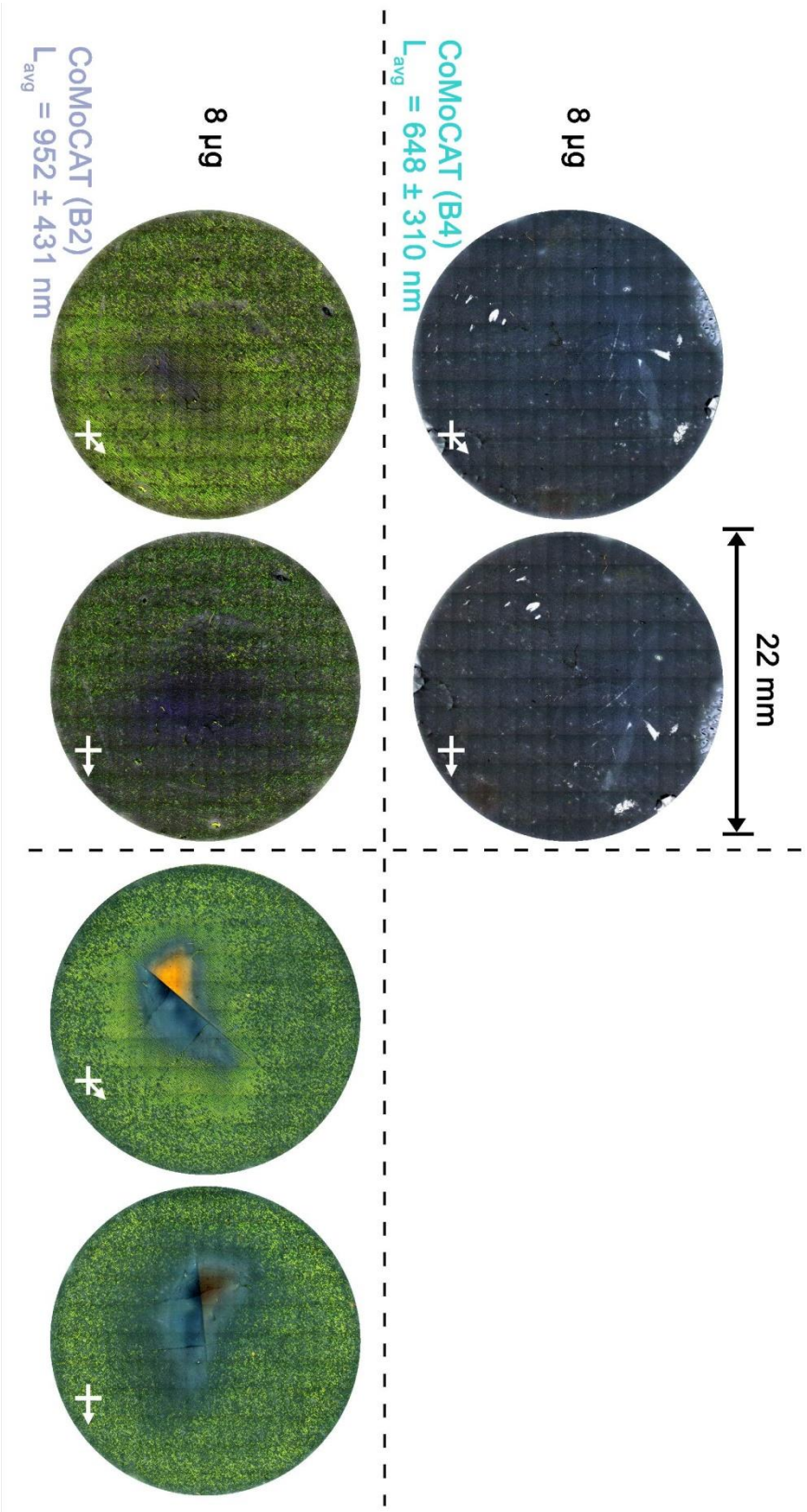

Figure S21. Cross polarized microscopy of CoMoCAT films from length fractions B2 and B4 in the bright (45°) and dark (0°) orientation and on pristine membranes.

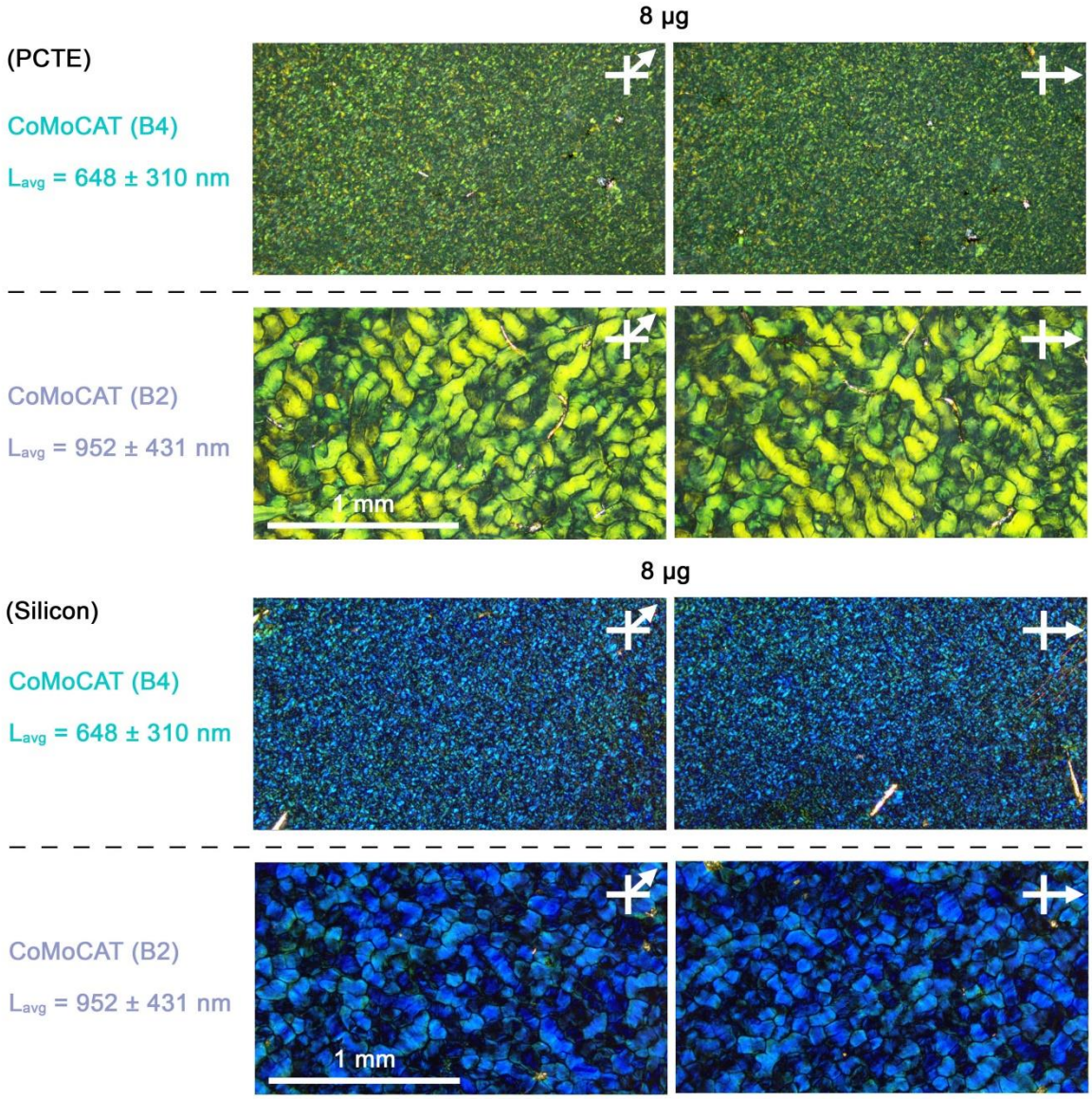

Figure S22. Cross-polarized light microscopy images of CoMoCAT films from 8 µg of the length-sorted fractions B4 and B2 in the bright (45°) and dark (0°) orientation. Images were recorded both on the membrane (top) and after transfer (bottom) of the SWCNT film to silicon.

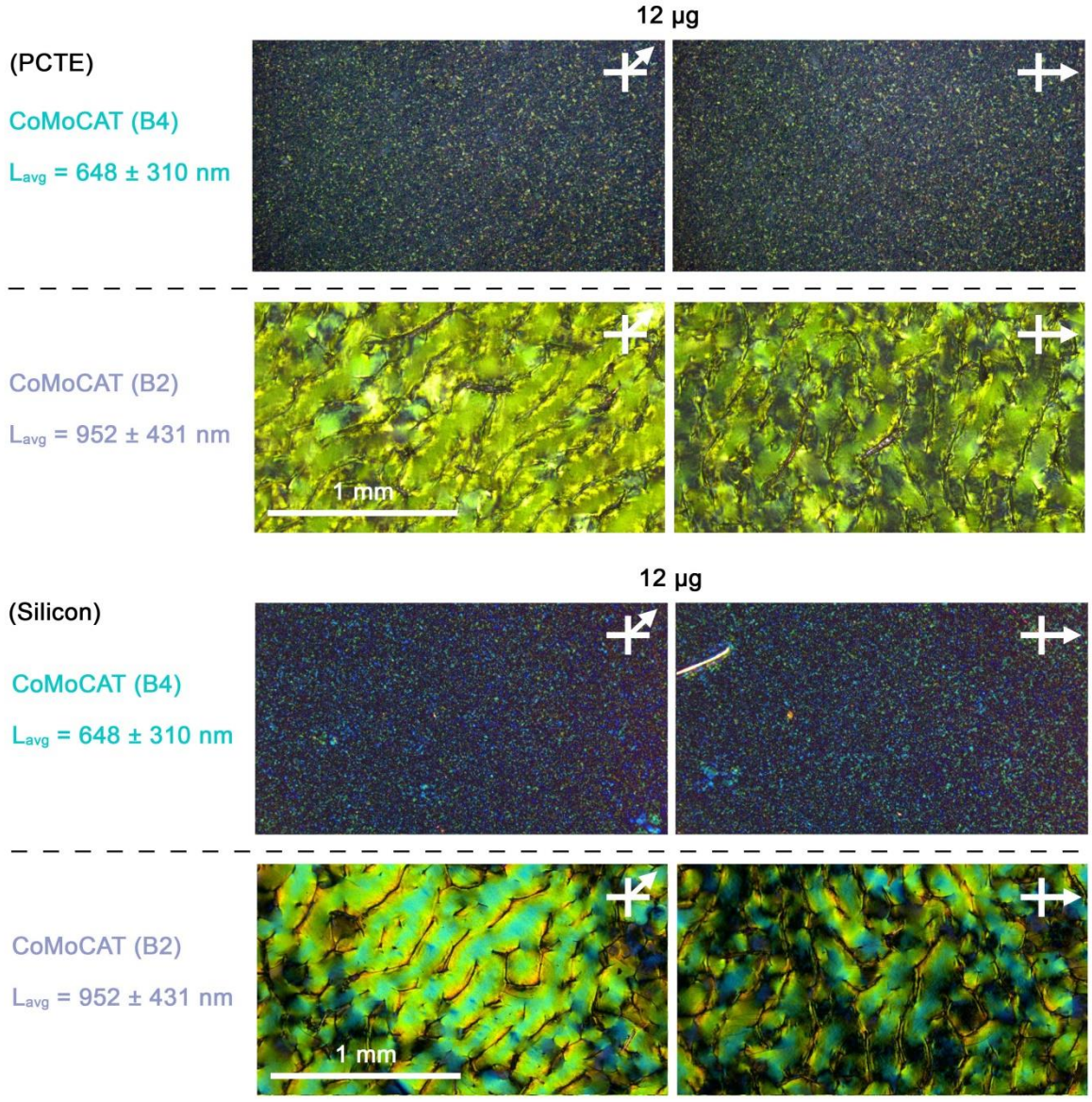

Figure S23. Cross-polarized light microscopy images of CoMoCAT films from 12 µg of the length-sorted fractions B4 and B2 in the bright (45°) and dark (0°) orientation. Images were recorded both on the membrane (top) and after transfer (bottom) of the SWCNT film to silicon.

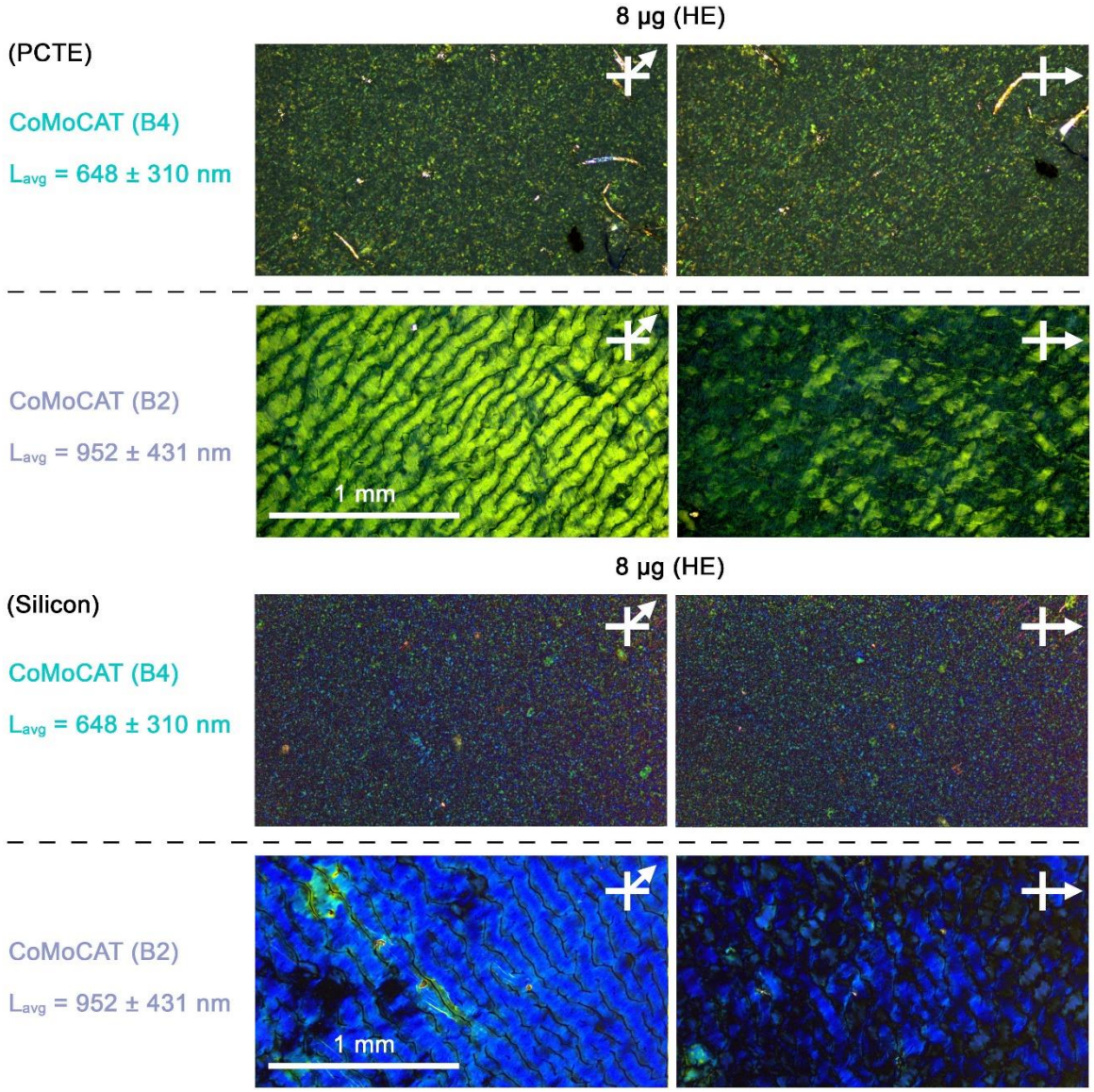

Figure S24 Cross-polarized light microscopy images of CoMoCAT films from 8 µg of the length-sorted fractions B4 and B2 in the bright (45°) and dark (0°) orientation and with the use of hot embossed membranes. Images were recorded both on the membrane (top) and after transfer (bottom) of the SWCNT film to silicon.

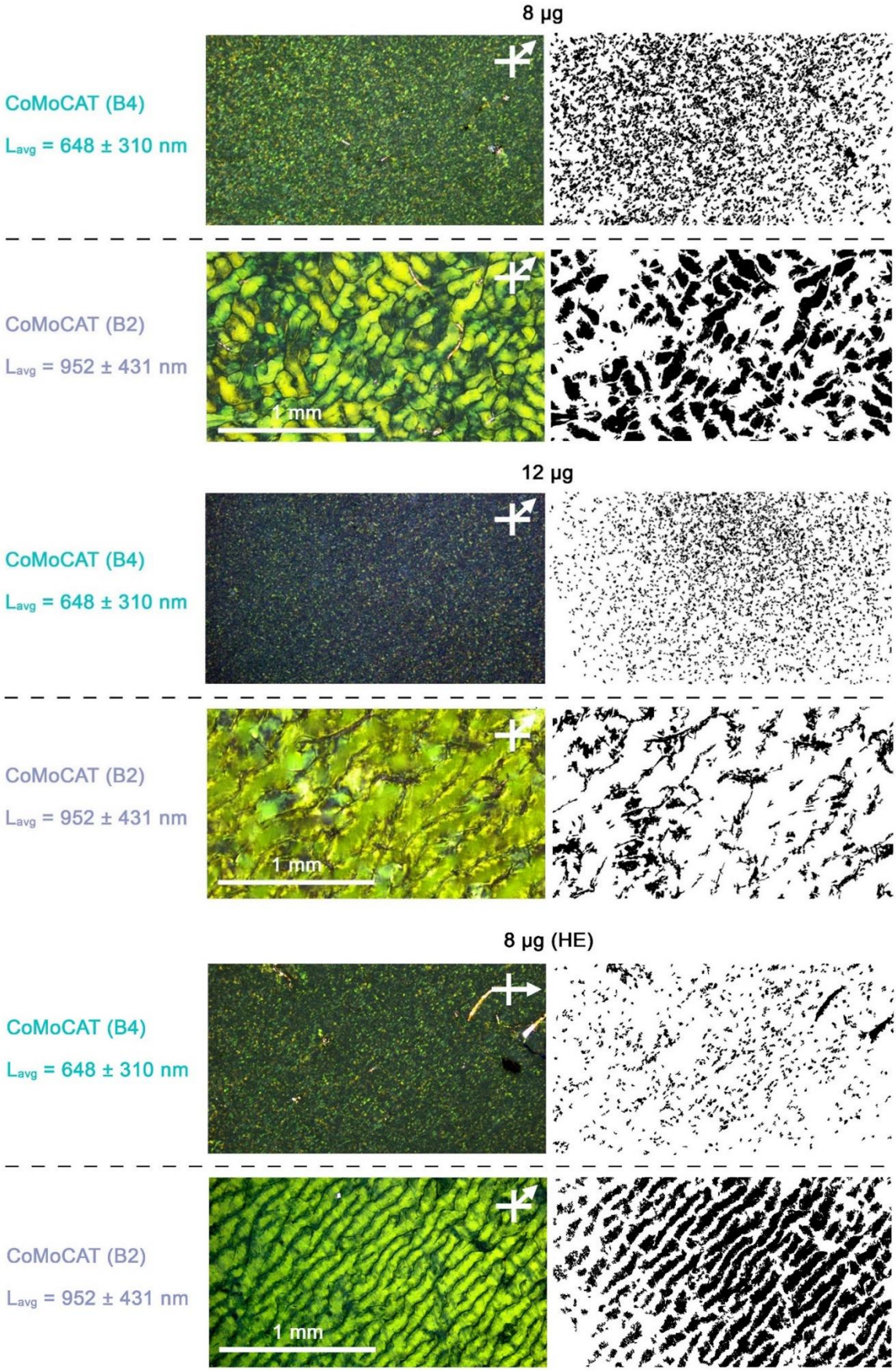

Figure S25. Cross polarized microscopy of CoMoCAT films from length sorted fractions B4 and B2 in the bright (45°) orientation and maps of the detected grains or grain boundaries (B2, 12 µg) using machine vision.

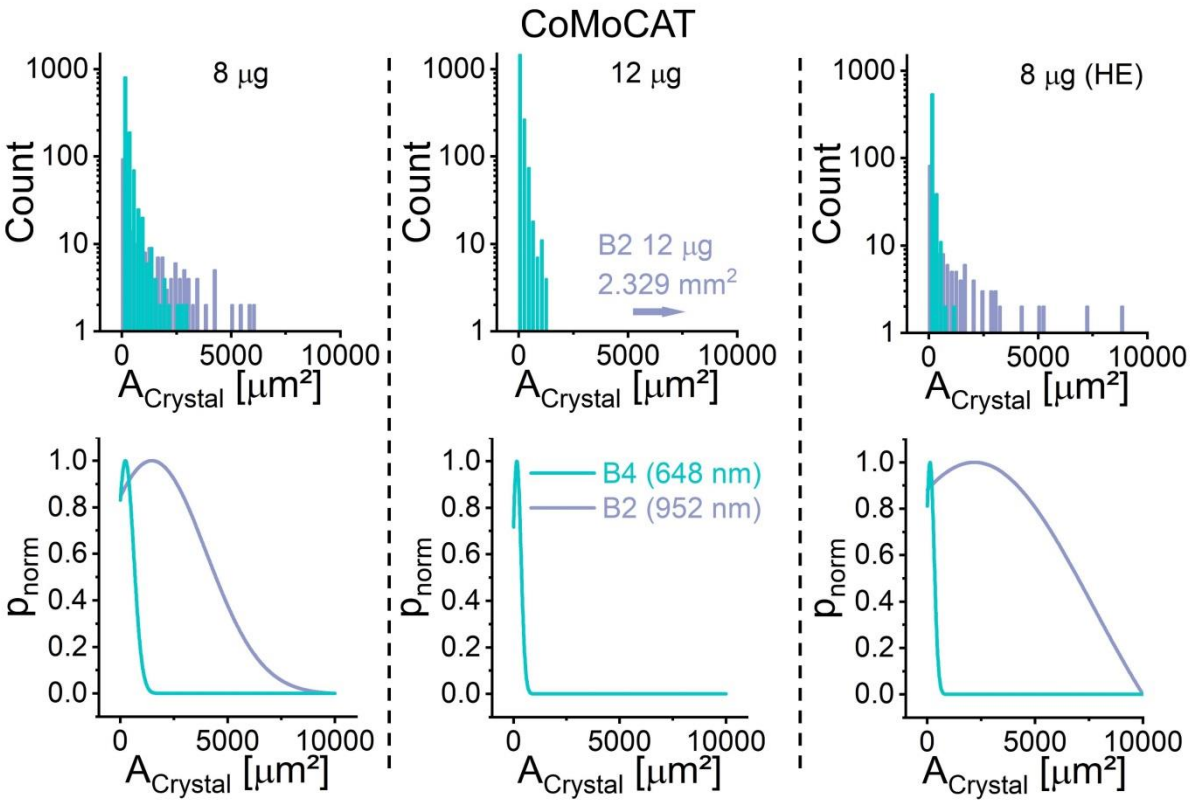

Figure S26. SWCNT domain size in CoMoCAT films from the length sorted fractions B4 and B2 as determined by machine-vision.

Figure S27. SEM images taken of the B2 CoMoCAT fraction filtered onto a hot-embossed 80 nm membrane shown in Figure 5 and Figure S24.

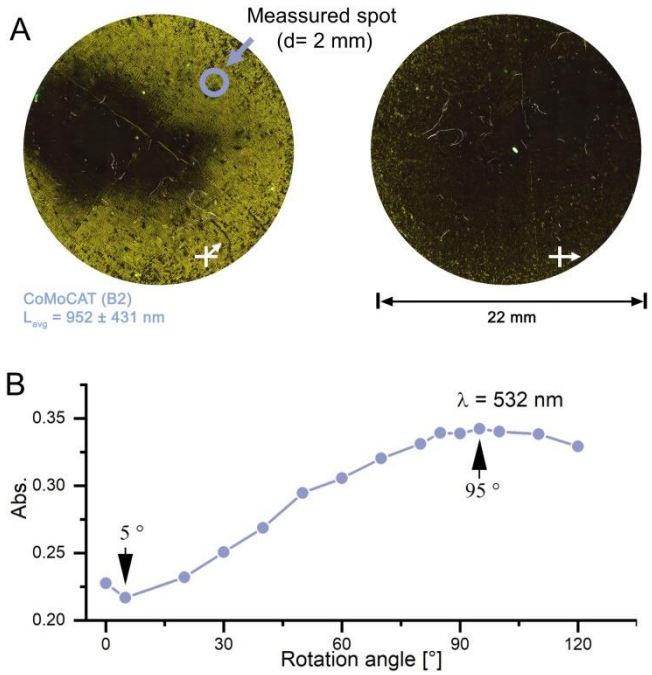

Figure S28. (A) CoMoCAT (B2) SWCNTs transferred from an HE membrane to an ITO-coated glass substrate, measured in transmittance using scanning cross-polarized light microscopy. The 2 mm beam spot for the angular dependent measurement shown in (B) is marked by a blue circle. The maximal and minimal absorption were measured at 5° and 95° using a wavelength of λ = 532 nm.

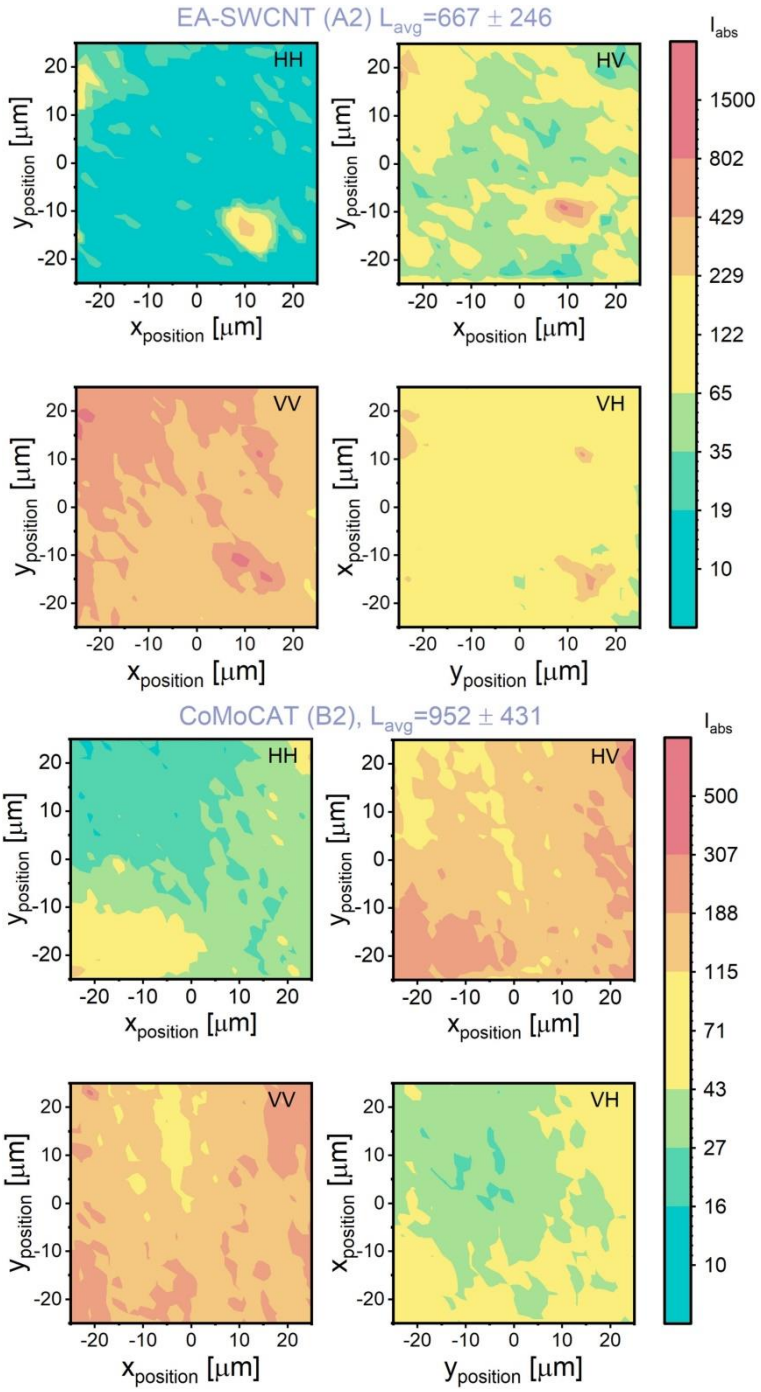

Figure S29. I_{HH}, I_{HV}, I_{VV} and I_{VH} measured to calculate the S_{2D} values shown in Figure 6 for films made with EA-SWCNT (A2) and CoMoCAT (B2).

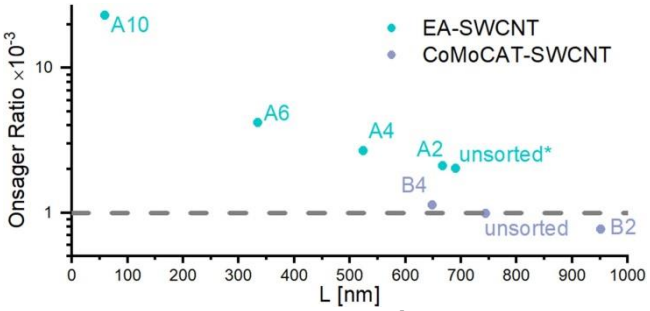

Figure S30. Logarithmic plot of the Onsager ratio $\frac{d_t}{L}$ with respect to length for the SWCNTs The threshold for alignment given by the considerations of Lagerwall *et al*. is plotted as a dotted line at $\frac{d_t}{L} = 1\times10^{-3}$.[1]

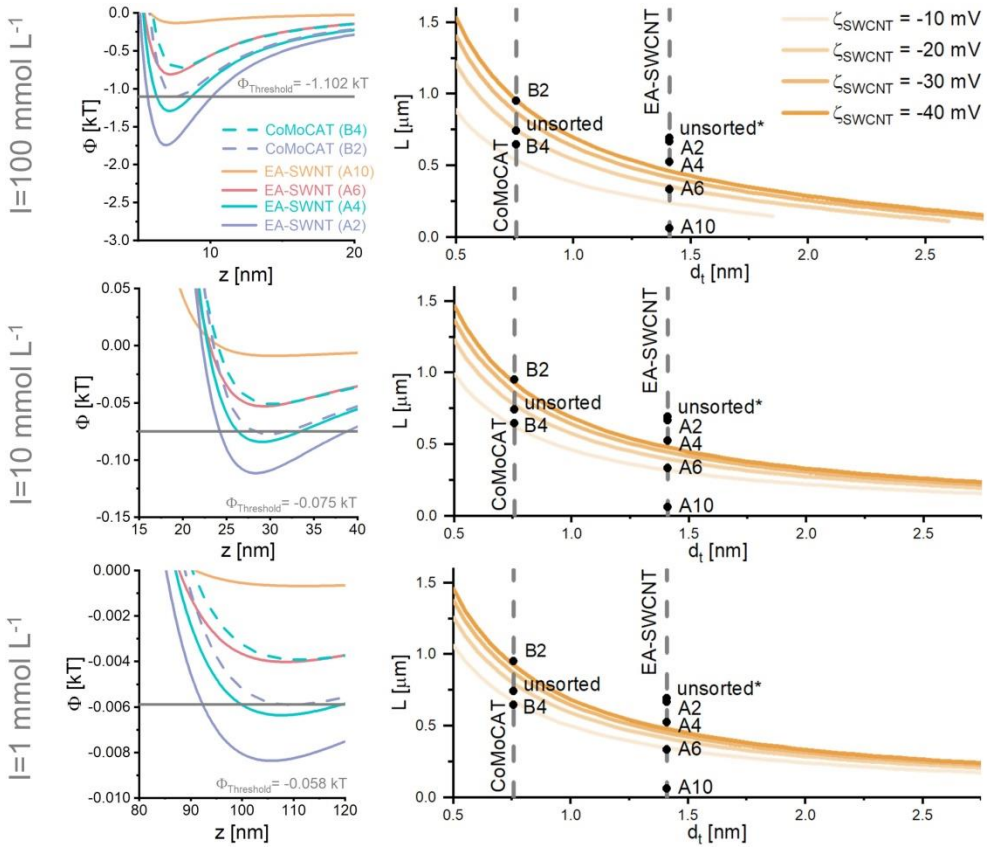

Figure S31. DLVO calculations for a variation of the ionic strength from bulk DOC (0.04 wt% DOC, $I =$ = 1 mmol L^{-1}) to I = 100 mmol L^{-1} with corresponding potential thresholds being defined as the secondary minimum of CoMoCAT (B2). Due to the enrichment of surfactant close to the membrane surface the real ionic concentration during filtration is unknown but it can be seen that the L(d) curves shown on the right, only differ for zeta potentials far away from the zeta potentials measured for the SWCNTs (cf. Figure 1, Figure S2).

References

[1] J. P. F. Lagerwall, G. Scalia, *J Mater Chem* **2008**, 18, 2890.